JOURNAL OF SOLID STATE CHEMISTRY 94, 368–380 (1991)

Porous Chromia-Pillared α-Tin Phosphate Materials

P. MAIRELES-TORRES, P. OLIVERA-PASTOR,*
E. RODRÍGUEZ-CASTELLÓN, AND A. JIMÉNEZ-LÓPEZ

Departamento de Química Inorgánica, Cristalografía y Mineralogía, Facultad de Ciencias, Universidad de Málaga, 29071 Málaga, Spain

AND A. A. G. TOMLINSON*

I.T.S.E., Area della Ricerca di Roma, C.N.R., C.P. 10 Monterotondo Stazione 00016 Rome, Italy

Received January 8, 1991; in revised form May 14, 1991

The reactions of $Cr(OAc)_3$ ($OAc^- = CH_3OCO^-$) solutions with colloidal suspensions of tetramethylammonium α-tin phosphate (α-$Sn[Me_4N]_{0.9-1.1}H_{1.1-0.9}(PO_4)_2 \cdot nH_2O$ = "Me_4N–SnP") have been investigated over a wide range of $[Cr(OAc)_3]$:$[Me_4N$–SnP] ratios, $Cr(OAc)_3$ concentrations, and heating conditions. On aging + reflux, Me_4N–SnP takes up oligomeric Cr^{3+} species to give crystalline, highly expanded materials having interlayer distances between 24 and 33 Å. Conversely, $Cr(OAc)_3$ solutions treated in the same way, but separately, and then added to colloidal Me_4N–SnP gave composites with little expansion (interlayer distance, d_{002} = 15 Å), collapsing to nonporous oxide-phosphates (d_{002} = 10 Å) on calcination. Separately polymerized $CrCl_3$/NaOH or $[Cr_3O(OAc)_6(OH_2)_3]^+$ (standard precursors in clay-pillaring) also gave poorly defined delaminated materials. Chemical, TGA/DTA, and visible/near UV spectroscopic evidence shows the intercalates are polyhydroxyacetato-Cr^{3+} species, and some may be formulated as $[Cr_3(OH)_6(OAc)]^{2+}$, $[Cr_4(OH)_7(OAc)^{3+}$, and $[Cr_5(OH)_7(OAc)_3]^{5+}$. They are formed *in situ* on the α-tin phosphate surfaces; possible orientations within the layers (taking into account the presence of zeolite-type water) is discussed. Calcination under N_2 at 400°C gives chromium oxide-pillared materials with d_{002} in the ranges 12.5–14.0 Å (from precursors prepared at higher Cr^{3+} concentrations) or 15–20 Å (from precursors at lower Cr^{3+} concentrations). The surface areas (BET, N_2, 77K): 264–386 $m^2\ g^{-1}$, compare well with analogues in clay chemistry (150–400 $m^2\ g^{-1}$). Pore-sized distributions (cylindrical pores model) are narrow, >70% of pores having widths <40 Å. Calcination in air leads to segregation of Cr_2O_3 which, after washing gives materials having wider pore-size distributions and lower surface areas. The ion-exchange properties of selected chromia-pillared materials with K^+, Co^{2+}, and Pr^{3+} have been investigated. The results are compared with models of porosity.

Introduction

The formation of porous, thermally stable materials by calcining intercalated polyhydroxy-cation precursors in layered solids, known as "pillaring," is an attractive means of obtaining acids with catalytic properties (*1*). Most work concerns smectite clays pillared by metal oxides, and chromia pillars have been particularly studied. In early work hydrolyzed Cr(III) solutions were used (*2*), but only recently have reproducible preparations of chromia-pillared smectites with high free heights (i.e., accessible height in the interlayer: interlayer distance–layer thickness) been re-

0022-4596/91 $3.00

ported (*3*). Manipulating the cavity–acidity characteristics in layered phosphates provides an alternative to smectite clays, and should lead to different materials characteristics. However, unlike smectites, layered phosphates require preswelling or colloidalization for precursor intercalation reactions to be successful (*4*). $[Me_4N]^+$ forms a stable colloid with α-$Sn(HPO_4)_2 \cdot H_2O$, of formula α-$Sn[Me_4N)_{0.9-1.0}H_{1.1-1.0}(PO_4)_2 \cdot nH_2O$ ("Me_4N-SnP"), which has recently been found to be useful for preparing intercalated Al_{13}–Keggin ion precursors (*5*). We here describe its use for obtaining chromia-pillared α-tin phosphates having porous structures with narrow pore-size distributions.

Experimental

Materials

Me_4N–SnP was freshly prepared as in Ref. (*5*). $[Cr_3O(OH_2)_3(OAc)_6]Cl \cdot 5H_2O$ was prepared by the method of Earnshaw *et al.* (*6*). Analysis: found C, 19.9; H, 5.2; Cl, 5.6; Cr, 21.1%; required for $C_{12}H_{36}ClCr_3O_{22}$: C, 19.9; H, 5.0; Cl, 4.9; Cr, 21.6%. Chromium(III) acetate was a Carlo Erba "pro analysi" product and was used as received. All other products were commercial products of the best available purity.

Intercalation of Cr(III) Species into α-Tin Phosphate

In preliminary experiments, aqueous $Cr(OAc)_3$ solutions were aged and/or refluxed separately and then added to Me_4N–SnP suspensions at 25°C. For all conditions, including very long reflux times, a material with d_{002} = 15 Å, collapsing on calcination at 200°C to a nonporous one having d_{002} = 10.3 Å, was obtained.

Direct reaction of aqueous $Cr(OAc)_3$ solutions with Me_4N–SnP suspensions under various conditions was then systematically explored using classical batch methods. Combining aging + reflux of the mixtures led to more ordered solids (high intensity d_{002} reflection in XRD, characteristic of layered phosphates). The uptake curve for $[Cr^{3+}]$: $[Me_4N$–SnP] mixtures varying between 11.6 and 276.9 meq Cr^{3+} added/g SnP_2O_7 submitted to reflux (1 day) is shown in Fig. 1. (Mixed "forcing" conditions, i.e., aging of the mixture at 25°C, followed by heating at 60°C, and then final reflux for 1 day, gave the same results.) Chromium concentrations in solution before and after uptake were monitored by colorimetry. After cooling the mixture, the solids corresponding to points 1–7 were filtered off (all were dirty green in color), washed well with water, air-dried, analyzed (C,H,N; TGA/DTA), calcined under air or nitrogen, and again analyzed. Analyses are listed in Table I.

The change in uptake with different chromium solution concentration was then followed in the region around points 4 and 5 of Fig. 1 (i.e., where *lower* [Cr(OAc)$_3$]:[Me_4N–SnP] ratios gave materials with *higher* chromium content and *higher* basal expansions). Samples 4a and 5a were separated and treated exactly as before. Subsequent work showed that refluxing for 4 days (to ensure complete polymerization) gave the same results.

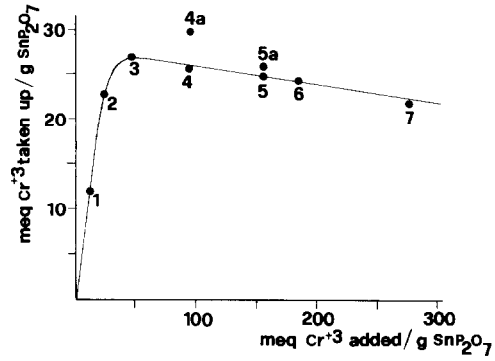

FIG. 1. Uptake of hydrolyzed $Cr(OAc)_3$ species by Me_4N–SnP. All points obtained under reflux for 1 day. Points 4a and 5a refer to Cr^{3+} solutions at lower concentrations (see text).

TABLE I

EXPERIMENTAL CONDITIONS FOR UPTAKE OF POLYHYDROXYACETATO-Cr^{3+} SPECIES BY "Me_4N–SnP" AND CHEMICAL ANALYSES OF MATERIALS SEPARATED ALONG THE UPTAKE CURVE OF FIG. 1

Sample	$[Cr^{3+}]^a$ (mol dm^{-3})	meq Cr^{3+} added/g SnP_2O_7	meq Cr^{3+} taken up/g $SnP_2O_7{}^a$	$d_{002}{}^b$ (Å)	$OAc^-/Cr^{3+}{}^c$	Suggested oligomer species	λ_{max} (nm)	d_{002} after calcination^d (Å)
1	0.02	11.6	11.5	—	0.25	—	—	—
2	0.03	23.1	22.8	26.5	0.35	$[Cr_3(OH)_6(OAc)]^{2+}$; (Cr_3)	593,424	14.0
3	0.05	46.2	27.0	31.4	0.46	(Cr_3) + (Cr_4)	590,419	—
4	0.10	92.3	25.5	27.9	0.51	$[Cr_4(OH)_7(OAc)_2]^{3+}$; (Cr_4)	589,414	13.9
5	0.17	153.2	24.6	26.3	0.55	—	—	—
6	0.20	184.6	24.1	24.9	0.57	(Cr_4) + (Cr_5)	588,420	13.8
7	0.30	276.9	21.7	23.9	0.61	$[Cr_5(OH)_7(OAc)_3]^{5+}$: (Cr_5)	588,423	12.5

[a] Determined from colorimetry (solutions) and flame photometry (solids).
[b] Determined from 3 orders of 00*l* basal spacing.
[c] C,H,N analyses and TGA (combustion to 950°C); no N present in all cases.
[d] Only d_{002}, d_{004} observable in XRD.

Contacting NMe_4–SnP suspensions with separately aged $CrCl_3$/NaOH solutions for various times and $[Cr^{3+}]$:[NMe_4–SnP] ratios (*2*), or contacting them freshly prepared $[Cr_3O(OH_2)_3(OAc)_6]Cl \cdot 5H_2O$ (5–180 meq g^{-1} exchanger), both common methods in clay chemistry (*7*), gave amorphous blue-green solids (*8*).

Selective Ion-Exchange Experiments

The pillared Cr–SnP in the Li^+ form (0.08 g) was suspended in mixed solutions of the metal acetate/lithium acetate of interest. Total concentration (2 × c.e.c.) and volume (25 ml) were maintained constant. Equilibrium concentrations in solid and in solution were deduced from changes in M^{n+} compared with initial solution concentration. Concentrations of metal ions in solution were determined by colorimetry (Co^{2+}, Pr^{3+}) or flame photometry (Li^+,K^+).

Chemical Analyses and Physical Measurements

Manipulations of solids were monitored by XRD (Siemens D501 diffractometer; graphite monochromator, Cu$K\alpha$ radiation) on powders and cast films. TGA and DTA were measured on a Rigaku Thermoflex (calcined Al_2O_3 as reference, 10°C min^{-1} heating rate) and Cr^{3+} was colorimetrically analyzed by the chromate method on alkaline solutions of samples (Kontron-Uvicon 810 spectrophotometer). Diffuse reflectance spectra were registered on a Shimadzu MPC 3100 spectrophotometer ($BaSO_4$ as reference). Adsorption–desorption of N_2 at 77 K was measured on a conventional volumetric apparatus. Samples were first degassed at 200°C overnight and adsorption–desorption of N_2 followed at 77.4 K.

Results

Heating and/or aging $Cr(OAc)_3$ and Me_4N–SnP together leads to expanded ordered intercalated precursors, not obtained if the $Cr(OAc)_3$ is first heated or aged. Under reflux conditions, Cr^{3+} uptake is rapid (up to 46.2 meq Cr^{3+} added/g SnP_2O_7) after which the amount of Cr^{3+} exchanged decreases smoothly (Fig. 1). This behavior is typical of an ion-exchange process occur-

ring simultaneously with a solution equilibrium, as described by Giles *et al.* (*9*). As the ion-exchange reaction proceeds, large oligomeric Cr^{3+} species are formed in solution which are too large to diffuse into the SnP matrix, but hinder exchange by smaller Cr^{3+} oligomers which become available. This model suggests that the species adsorbed are in a narrow range and well-defined, in agreement with variations in Cr^{3+} concentration in the contact solution. It also agrees with the chemical analyses and TGA/DTA of the materials separated at points 2–7, and in particular points 2, 4, and 7.

Further evidence that the species intercalated are well-defined species is the fact that the materials separated at points 1–7 of the uptake curve are phase pure; there is no evidence for more than one basal (d_{002}) XRD peak. All have XRD still characteristic of crystalline layered structures with narrow d_{002} peaks (although $00l$ progressions are visible only to $l = 3$). Low-loaded species (point 1 in Table I) are an exception, giving amorphous products on calcination, even at temperatures as low as 200°C, and will not be discussed further.

Instead, the precursor-intercalation methods used for smectites indicate that more than one species intercalates. The uptake of $[Cr_3O(OH_2)_3(OAc)_6]^+$ by Me_4N–SnP is non-Langmuir in type, presumably because partial hydrolysis of the Cr^{3+} cluster in solution leads to a range of oligomers, in turn providing only amorphous particles consisting of short-range order intercalated "packets" (still considered as "pillared" by some authors (*10*)). Brindley and Yamanaka's method (*7*) also fails, because at equilibrium the Cr^{3+} solution pH of 2.5 is too acidic for exchange kinetics conditions required by layered phosphates (*11*).

The Cr^{3+} content in materials 4 and 5 *increases* as solution Cr^{3+} concentration *decreases*. For example, when $Cr(OAc)_3$ corresponding to 92.3 meq Cr^{3+}/g SnP_2O_7 is

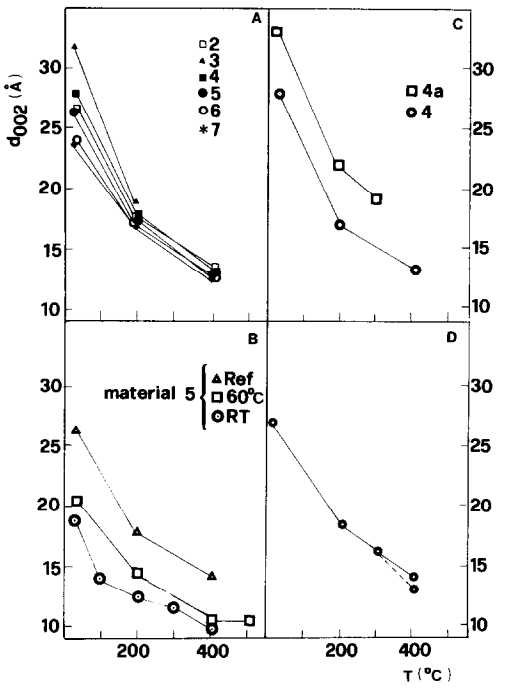

FIG. 2. (A) Interlayer distances of materials 2–7 of Fig. 1 and their behavior on calcination in air. (B) XRD basal spacings and their thermal behavior for intercalate precursors prepared from hydrolyzed solutions with $[Cr^{3+}]$ in external solution of material 5, at different temperature. (C) XRD basal spacings and their thermal behavior of materials 4 and 4a. (D) XRD basal spacings of material 5a (note presence of two phases).

diluted twice, the Cr^{3+} taken up increases from 25.5 to 29.7 meq Cr^{3+}/g SnP_2O_7 (see Table I). Figure 2 also shows the XRD for these materials. The following points are of importance:

(i) d_{002} values are very similar for precursor solutions aged at 25°C or 60°C alone (B);

(ii) d_{002} are much higher for reflux conditions (24–25 Å) than for aging at 25 and/or 60°C (19–21 Å) alone (A);

(iii) for more forcing reflux conditions, higher dilutions lead to materials with higher interlayer distances (d_{002} = 27–32 Å) (C,D);

(iv) calcination—in either air or N_2—leads to varying decrease of the interlayer

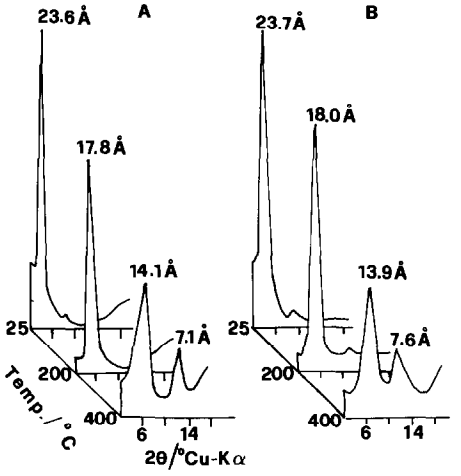

FIG. 3. Typical XRD; material 4 of Fig. 1 (film). (A) before and after calcination in N_2; (B) before and after calcination in air.

distance, the highest final interlayer distances being obtained for materials from more dilute solutions;

(v) the calcined materials retain layered structures.

The crystallinity of these precursor materials is high (see Fig. 3 for a typical example). However, calcination in air leads to formation of an impurity phase (probably α-SnP) and also—as expected—to formation of considerable amounts of dichromate ion (from optical spectrum, after washing well with deionized water). This presumably derives from segregated Cr_2O_3 (characteristic XRD reflexions observed at $T > 500$°C); its presence led to higher apparent surface areas when materials were not washed first. Calcination under N_2 gave practically no detectable dichromate washings. All porosity and ion-exchange results refer to calcined samples first washed well with water.

A typical TG/DTA analysis (material 4a) is shown in Fig. 4 (2–7 gave analogous results). Water is lost up to ca 230°C (in two steps, the first from hydration-shell and

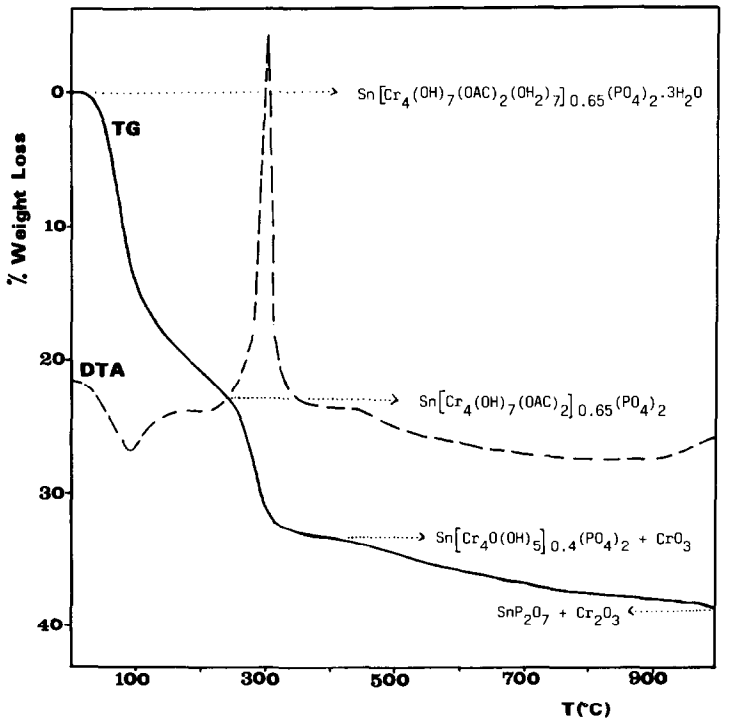

FIG. 4. Typical TGA/DTA analysis; material 4, with decomposition pathway.

pseudozeolitic water and the second probably from condensation reactions occurring in the oligomer intercalate). Combustion of organic residues (acetate groups, from chemical analysis and IR spectra) occurs between 230 and 350°C (i.e., the precursors themselves are relatively thermally stable). The exotherm for acetate combustion lies at 341–342°C in materials prepared at 25°C and 60°C, whereas in refluxed samples it lies at 300°C, clear evidence that the interlayer precursor species is different in the two cases. There was no clear evidence for the characteristic endotherm—expected at 430–460°C—due to the phosphate → pyrophosphate condensation, nor was there an exotherm expected at 800–900°C for a layered SnP_2O_7 → cubic SnP_2O_7 transition (*12*).

Several chemical tests were carried out on the materials:

(i) All precursor materials gave only partial exchange–elution of oligomer on suspension in 0.2 mol dm^{-3} HCl (Al–Keggin ion analogues are completely eluted from naturally occurring silicates under these conditions (*13*)). This indicates that the polyhydroxyacetato-Cr^{III} moieties interact more strongly with the phosphate layers.

(ii) A sample containing 25.5 meq Cr^{3+}/g SnP_2O_7 was calcined under different conditions and contacted with hot water (60°C) for 1 day and the washings were analyzed for Cr^{3+}. The extractable Cr^{3+} was: 1.35% (as prepared), 45.0% (calcined in air at 400°C), 25.7% (calcined in air at 500°C), and 7.7% (calcined under N_2 at 400°C).

(iii) After calcination and thorough washing, no remaining Cr^{3+} species could be extracted with either 0.2 mol dm^{-3} HCl or transition metal ion-containing solutions. This provides indirect evidence that there is bonding between chromia moieties and phosphate layers, further corroborated by the fact that no calcined products could be swelled with ethyleneglycol (commonly used in past clay studies (*14*) as a criterion for swellability).

Figures 5 and 6 show the results of ion-exchange selectivity experiments using calcined materials 2 and 4. The ion exchange of Li^+ with M^{n+} ions may be expressed as

$$n\text{Li(PLP)} + M^{n+} \rightarrow M(\text{PLP})_n + n\text{Li}^+,$$

where (PLP) is the formula weight of the "pillared layered phosphate" containing 1.6 eq of exchange. The reaction is described by a selectivity coefficient $K_{Li^+}^{M^{n+}}$:

$$K_{Li^+}^{M^{n+}} = \frac{\overline{[M^{n+}]}(Li^+)^n}{\overline{[Li^+]}^n(M^{n+})},$$

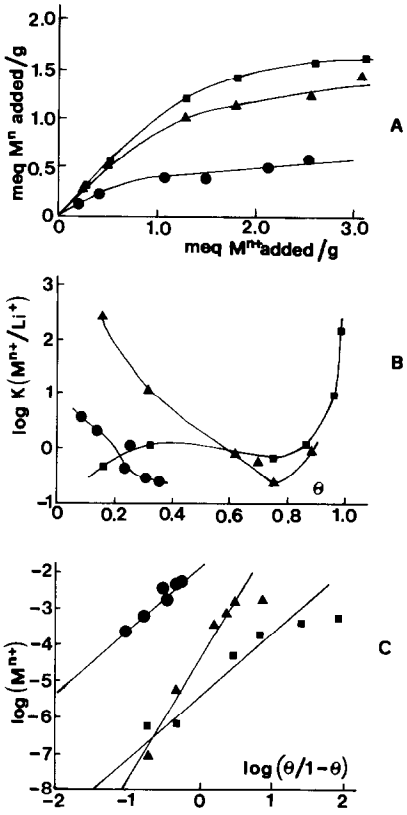

FIG. 5. (A) Exchange isotherms for K^+(●), Co^{2+} (▲), and Pr^{3+} (■) on the material 2 exchanged with Li^+ after calcination at 400°C under N_2. (B) Relationship between surface ion composition of the M^{n+}/Li–Cr–SnP and the selectivity coefficient $K_{Li^+}^{M^{n+}}$. (C) Relationship between the M^{n+} adsorption function, $\theta/1-\theta$, and the solution activity of M^{n+} for Li^+/M^{n+}.

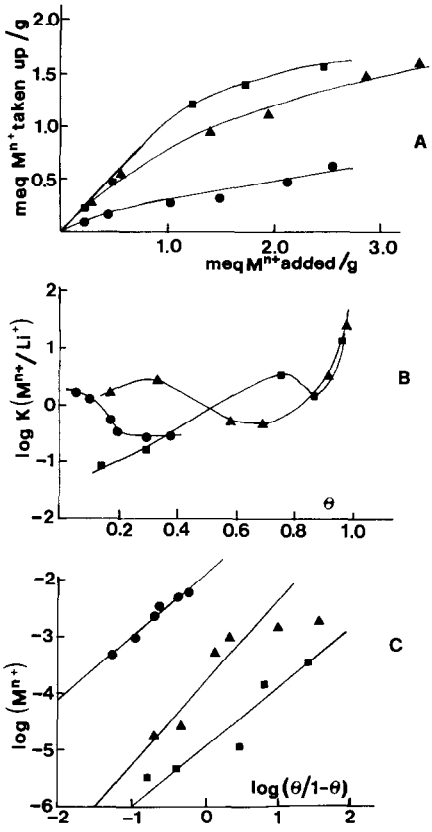

FIG. 6. As for Fig. 5; Calcined, Li^+-exchanged material 4.

where the bar represents ions in the adsorbed phase, square brackets the equivalent fractions in the solid, and parentheses the ion activities in solution phase. The c.e.c. of both Li^+-exchanged forms is 1.6 meq/g exchanger. The McBride and Bloom Langmuir-type equation for describing adsorption of M^{n+} ions on clays (*15*) has been utilized, in which the activity of M^{n+} in solution is a function of the coverage, θ, of the phosphate surface by M^{n+}:

$$(M^{n+}) = K(\theta/1 - \theta)x,$$

where K and x are constants and θ the equivalent fraction in the solid. In this model of ion exchange, the strong adsorption of high-charge ions is a result of the entropy gain connected with water disorder or with an increase in ion disorder at the exchange sites (*16*). Fits of the log (M^{n+}) vs log $(\theta/1 - \theta)$ plots to the McBride–Bloom equation gave the parameters

	Material 2		Material 4	
	K	x	K	x
Li^+/K^+	1.8×10^{-2}	1.844	1.3×10^{-2}	1.146
Li^+/Co^{2+}	1.7×10^{-4}	1.461	4.3×10^{-5}	3.480
Li^+/Pr^{3+}	3.2×10^{-5}	1.667	1.2×10^{-5}	0.974

The adsorption–desorption isotherms for N_2 are all of type IV in the BDDT classification (Fig. 8); i.e., they are characteristic of mesoporous materials with microporous contributions (*17*), as inferred from the adsorption values in the low relative pressure region. Micropore volumes were calculated from α_s methods (*17*).

Discussion

Intercalate Precursor Species

Whether or not pillared materials find uses in the future, identification of precursor intercalates remains a major unsolved issue. The large Keggin-type polyhydroxyaluminum ("chlorhydrol") (*1*) and polyhydroxy chromium(III) (*2, 7*) used to date are formed *ex situ*. Problems arise due to the presence of solution equilibria (*18*), and to large variations in local concentrations of base (with metal hydroxide precipitation) and parallel exchange reactions with surface groups (e.g., the Na^+ ions from NaOH used for polymerizing $CrCl_3$). These may lead to both lateral disordering effects during intercalation and irreproducible stuffing of interlayers. By contrast, the hydrolysis of $Cr(OAc)_3$ *in situ* on the colloidal surfaces of Me_4N–SnP, which exploits the kinetic robustness of Cr^{3+} with no complications by redox processes during intercalation and

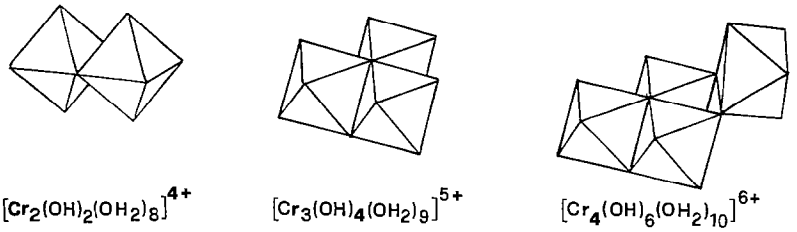

SCHEME 1. Connectivities of Cr^{3+} octahedra in aqueous polyhydroxy-Cr^{3+} species reported in the literature (*20, 23*).

buffering by OAc^- ions, provides an apparently cleaner route to porous solids.

Chemical identification is straightforward: the precursors are polyhydroxyacetate-Cr^{3+} species, having chain lengths which differ depending on aging–heating regime and concentration. The more promising ones, in terms of interlayer expansion are those at points 2, 4, and 7 of the uptake curve, formulated as

material 2:

$$\alpha\text{-Sn}[Cr_3(OH)_6(OAc)(OH_2)_6]_{0.8}H_{0.4}(PO_4)_2 \cdot H_2O;$$

material 4:

$$\alpha\text{-Sn}[Cr_4(OH)_7(OAc)_2(OH_2)_7]_{0.67}(PO_4)_2 \cdot 3H_2O;$$

material 7:

$$\alpha\text{-Sn}[Cr_5(OH)_7(OAc)_3(OH_2)_8]_{0.38}H_{0.1}(PO_4)_2 \cdot 4H_2O$$

(water molecules included for analytical balance and to give six-coordinate Cr^{3+}). Points 3, 5, and 6 represent materials containing mixtures of oligomers.

Structural conclusions are more uncertain, although comparison with studies of the early stages of aquochromium^{3+} polymerization in solution (*19–22*) seems reasonable (there are no comparable studies with acetate-containing species). Dimers to tetramers have been most clearly identified (*19, 20*), both being major species at pH 4 (*21*). They have edge-shared "closed" structures (Scheme 1), although the dimer also gives an open form (*22*), and the tetramer has an even more closed form (formed after deprotonation (*23*), which is unlikely in the present pH conditions). Further, Stünzi and Marty (*23*) used an empirical spectral criterion $\varepsilon_1/\varepsilon_2$ (1.17-monomer; 1.18 = dimer; 1.6-trimer; 1.95 = tetramer, and 1.5–1.6 = pentamer and hexamer) to distinguish between these structures. This criterion appears to be related to the connectivity between octahedra; the higher the connectivity, the higher is ε_1 with respect to ε_2 (ε_1, ε_2 are the molar absorbances of bands $\nu_1(^4T_{2g} \leftarrow {}^4A_{2g})$ and $\nu_2(^4T_{1g} \leftarrow {}^4A_{2g})$).

In materials 2–7 and 5a, $\varepsilon_1/\varepsilon_2$ = ca 1.18–1.2, from which we conclude that linear edge-shared oligomers are present, rather than the closed ones of Scheme 1. (The electronic spectra of 3 and 5 show evidence for broadening of both bands compared with those for 2, 4, and 7). IR spectra confirm that acetate ions are present, and they are characteristic of bidentate $MeCO_2^-$ groups rather than ionic ones, as expected. This is also supported by the fact that ν_2 in the electronic spectra decreases in wavelength compared with the spectra of both $Cr(OAc)_3$ itself (ν_2 446, ν_1 590) and $[Cr_3O(OH_2)_3(OAc)_6]^+$ (ν_2 448, ν_1 611 nm) (Fig. 7).

It is not possible to construct a suitable stereomodel and fit it into the interlayer space, as often done in intercalation chemistry (*24*), because large amounts of struc-

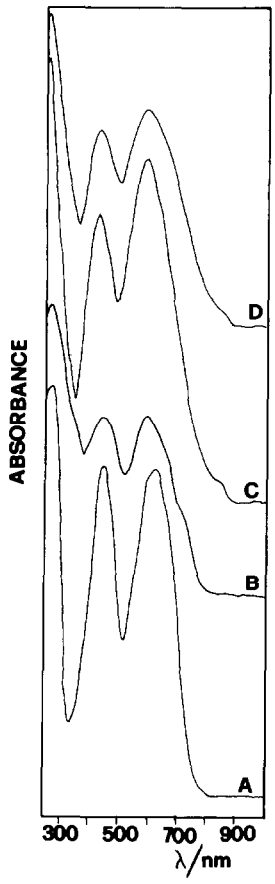

FIG. 7. Diffuse reflectance spectra. (A) $[Cr_3O(OH_2)_3(OAc)_6]Cl \cdot 5H_2O$; (B) $Cr(OAc)_3$; (C) 4 (25°C aged); (D) 4 (25°C/60°C, aged, then refluxed).

tural water are present. This causes the considerable interlayer collapse after dehydration at 200°C, to give materials with a much lower free height (taken to be d_{002} − 6.5 Å, the approximate layer thickness (*25*)) and in narrow ranges: 17–19 Å (materials 2–6) and 21–21.5 Å (materials 4a, 5a). There are three possibilities (Scheme 2), one of which (ii) may be eliminated immediately (removal of zeolitic water would lead to no collapse).

TABLE II

TEXTURAL PARAMETERS FOR MATERIALS 2–5

Material	Calcination temp.	S_{BET}	C_{BET}	Σs^a	$\Sigma V_{ac}{}^a$	$d_p{}^a$	$V_{micro}{}^b$
2	400 (N_2)	267	98.8	287	0.247	37	0.088
4	400 (N_2)	386	132.6	416	0.324	34	0.115
4a	400 (air)	236	84.5	272.4	0.284	84	0.040
	400 (N_2)	288	237.9	263.6	0.222	30.8	0.107
5a	400 (air)	242	242.9	233.3	0.212	35.0	0.101
	400 (N_2)	264	437.9	188.2	0.145	21.9	0.107

[a] Parameters as defined and calculated in Cranston and Inkley (*28*).
[b] Using α_s plot (*17*).

Assuming that there is no large movement of the oligomer inside the layer on dehydration (such as, for example, tilting) would argue against form (iii) (the rigid rodlike oligomers would be expected to give a higher interlayer distance on removal of cavity water).

Chromia Pillars

Calcination of materials 2–7 subsequently occurs with less precipitous collapse in interlayer distance, and all remain crystalline up to 400°C. More importantly, surface areas are quite high, ranging between 200 and 380 $m^2\ g^{-1}$ (Table II). (The theoretical surface area for a pillared α-tin phosphate is expected to be 850 $m^2\ g^{-1}$, assuming the basal structure is similar to that in α-zirconium phosphate (*5*)). This again argues for the presence in the precursors of

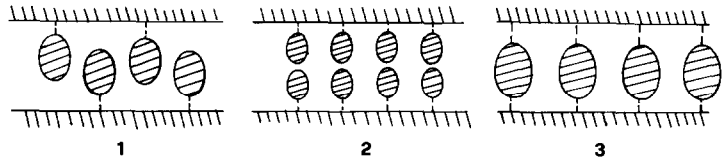

SCHEME 2. Possible orientations of oligomers between the layers in the precursors (schematic).

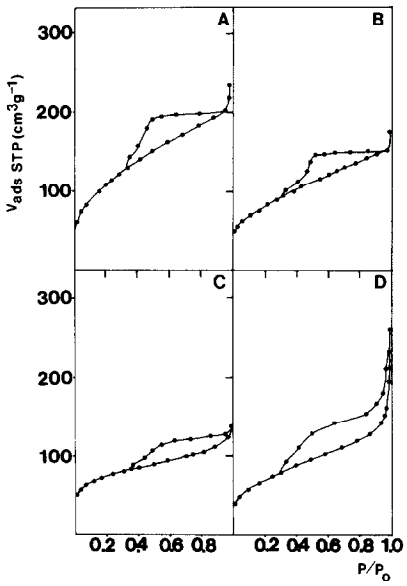

FIG. 8. Adsorption–desorption isotherms of (A) material 4 calcined at 400°C under N_2; (B) material 4a calcined at 400°C under N_2; (C) material 5a calcined at 400°C under air, and (D) material 5a calcined at 400°C under N_2.

relatively ordered interlayer oligomer organization, as in Scheme 2. The surface areas compare well with those obtained to date for pillared clays (*26*) and are much higher than those reported in a study of $Cr(OAc)_3$ intercalated in α-$(Zr\ PO_4)_2HNa \cdot 5H_2O$, in which surface areas of ca 40 $m^2\ g^{-1}$ for calcined materials were imputed to "stuffing" of the interlayer by fragments (*27*). As shown in Table II, the decrease in surface area on calcining in air (rather than N_2) may also be due to some blocking of the cavities formed, but this was never sufficient to cause complete porosity removal.

The textural parameters were derived from the cylindrical pore model (*28*), and applying "*t*" plots (*29*) and the α_s method (*17*), as before (*5*), for assessing microporosity. The pore-radius distributions obtained lie in a relatively narrow range for all four materials examined: 8–15 Å (see Fig. 9); this is as narrow as that found for porosity induced by derivatization of phosphate groups with phosphonates (*30*).

Note that, although the increase in average pore diameter with increase in the amount an size of chromium oligomer precursor agrees with the increase in pillar height, there does not appear to be a simple relation between the latter and surface area.

An objection is that the pore distributions represent mesoporosity induced by cavities formed by "packets" of layers (i.e., limiting small particles) becoming associated in an end-side fashion to give almost triangular pores, rather than by pillaring (*6, 31*). (The literature on porous solids is replete with examples of materials giving pores classified as "mesopores" in the width range $2r_p$ = 15–40 Å (*32*); others classify these as micropores (*1*)). A typical SEM micrograph (Fig. 10) shows considerable

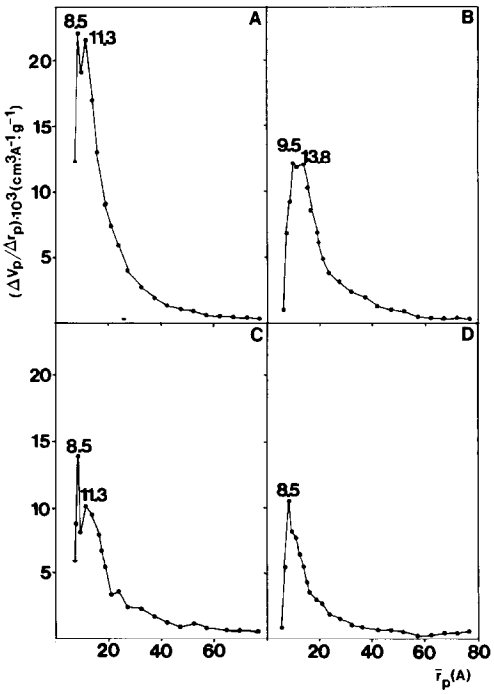

FIG. 9. Kelvin pore-radius distributions of materials. Details as in the legend to Fig. 8.

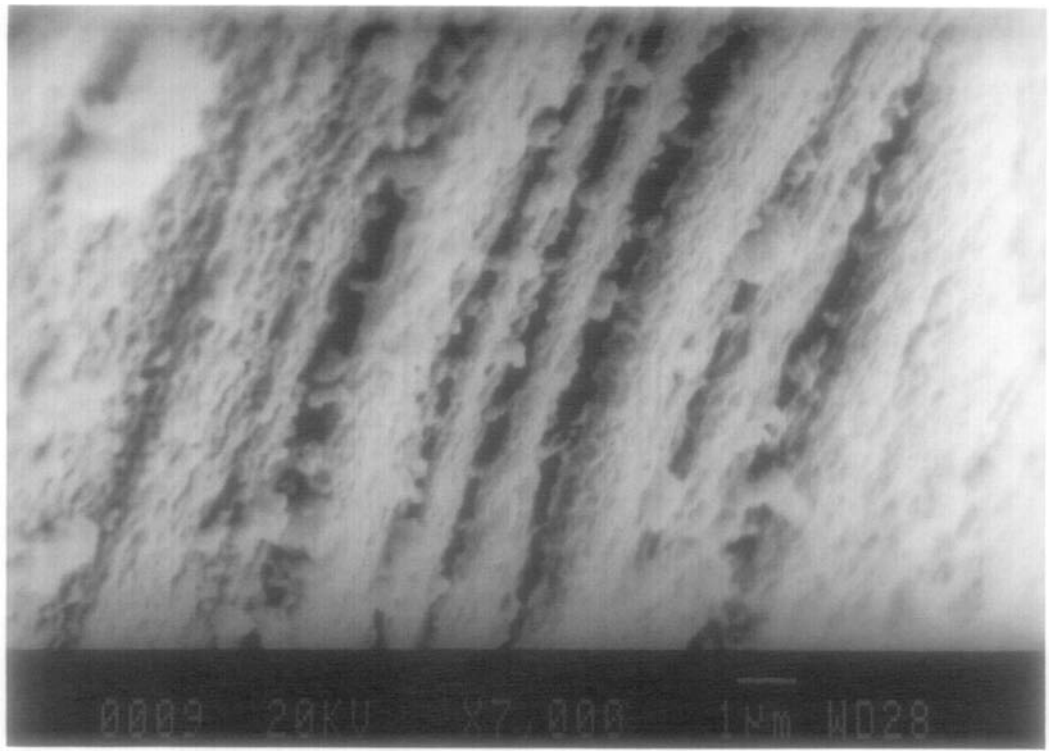

FIG. 10. SEM micrograph of Cr–SnP, material 4.

macroporosity and the presence of mesopores. However, the latter appear always to be restricted to within the packets of layers. Further, we note from Fig. 9 that air-treated materials have broader, more inhomogeneous, pore-size distributions, which is as expected for a "thinning out" of chromium oxide pillars, but is not easily rationalized on the interpacket pore model. We conclude that the porosity is indeed induced by pillaring (and it seems highly unlikely that aggregation of packets would occur in so homogeneous and reproducible a fashion as to give rise to such narrow pore-size distributions).

The ion-exchange results support this view: c.e.c.s are too high to be due to surface exchange alone. There is, however, no obvious relationship between surface area and c.e.c. (Note that these materials present cation-exchange properties alone, differently than pillared clays, which show both anion and cation exchange (*33*). In a rigid system, as expected to occur in a pillared material with high available internal space (recall pores with radii of 8.5 and 11.2 Å) accommodation of highly mobile ions and hydrated cations is to be expected, i.e., exchange effectiveness is directly related to the charge/radius ratio of the M^{n+} cations. There is nonlinearity in the log (M^{n+}) vs log $(\theta/1 - \theta)$ plots (especially for Co^{2+}) (*16*), and thus, heterogeneity of the internal exchange sites may account for the composition-dependent selectivities. We conclude that there are different accessibilities of the internal surface of these materials to N_2 molecules (possibly reflected in the high C_{BET} parameters) and hydrated cations.

Clearly, considerations of pore geometry

should also take into account other factors, such as the volume of the exchanged cation, the size and shape of the pores, structural rigidity, and accessibility of layer or pillar to N_2, which must await further structural information.

Conclusions

Colloidally dispersed, buffered α-tin phosphate surfaces provide a good medium for obtaining well-ordered Cr^{3+}-oligomers as precursors for preparing chromia-pillared layered phosphates. The accessible colloidal surface permits growth of polyhydroxyacetate-Cr^{3+} oligomers in an ordered way, which on calcination give rise to porous oxide-pillared materials of narrow pore range. Further work is under way to assess how general the method is, and to resolve ambiguities in interpretation of pore radii.

Acknowledgments

We thank the EEC (Euram Project I-0027) and C.I.C.Y.T. (Project No. MAT90-298) for financial support.

References

1. D. E. W. Vaughan, *in* "Catalysis Today" (R. Burch, Ed.), p. 187, Elsevier (1988); D. E. W. Vaughan, R. J. Lussier, and J. S. Magee, U.S. Patent 4,176,090 (1979); G. Poncelet and A. Schultz, *in* "Chemical Reactions in Organic and Inorganic Constrained Systems" (R. Setton, Ed.), p. 165, Riedel, Amsterdam (1986)
2. G. W. Brindley and S. Yamanaka, *Am. Mineral.* 1979, **64,** 830 (1979); M. Carr, *Clays and Clay Miner.* **3,** 357 (1985); P. Rengasamy and J. M. Oades, *Aust. J. Soil Res.* **16,** 53 (1978).
3. M. S. Tzou and T. J. Pinnavaia, *in* "Pillared Clays, Catalysis Today" (R. Burch, Ed.), p. 243 (1988).
4. A. A. G. Tomlinson, in "Pillared Layered Structures. Current Trends and Applications" (I. V. Mitchell, Ed.), p. 91, Elsevier Applied Science, London (1990).
5. P. Olivera-Pastor, A. Jimenez-Lopez, P. Maireles-Torres, E. Rodriguez-Castellon, A. A. G. Tomlinson, and L. Alagna, *J. Chem. Soc. Chem. Commun.*, 751 (1989); P. Olivera-Pastor, A. Jimenez-Lopez, P. Maireles-Torres, E. Rodriguez-Castellon, A. A. G. Tomlinson, and L. Alagna, *J. Mater. Chem.*, 319 (1991).
6. A. Earnshaw, B. N. Figgis, and J. Lewis, *J. Chem. Soc. A*, 1656 (1966).
7. S. Yamanaka, T. Doi, S. Sako, and M. Hattori, *Mater. Res. Bull.*, **19,** 161 (1984); M. A. Martin-Luengo, H. Martins-Corvalho, J. Ladriere, and P. Grange, *Clay Miner.* **24,** 495 (1989).
8. P. Maireles Torres, P. Olivera Pastor, E. Rodriguez Castellon, A. Jimenez Lopez, and A. A. G. Tomlinson, in "Pillared Layered Structures" (I. V. Mitchell, Ed.), p. 137, Elsevier Applied Science, London, 1990.
9. C. H. Giles, T. H. McEwan, S. N. Nakhwa, and D. Smith, *J. Chem. Soc.*, 3973 (1960).
10. K. Suzuki, T. Mori, K. Kawase, H. Sakani, and S. Iida, *Clay Miner.* **36,** 147 (1988).
11. U. Costantino and A. Gasparoni, *J. Chromatogr.* **51,** 289 (1970).
12. A. La Ginestra and P. Patrono, *Mater. Chem. Phys.* **17,** 161 (1987).
13. V. C. Farmer, B. F. L. Smith, M. J. Wilson, P. J. Loveland, and R. W. Payton, *Clay Miner.* **23,** 271 (1988).
14. D. H. Doff, N. H. J. Gangas, J. E. M. Allan, and J. M. Coey, *Clay Miner.* **23,** 361 (1988).
15. M. B. McBride and P. R. Bloom, *Soil Sci. Soc. Amer. J.* **41,** 1073 (1977).
16. M. B. McBride, *Clays Clay Miner.* **28,** 255 (1980).
17. S. J. Gregg and K. S. W. Sing, "Adsorption, Surface Area and Porosity," Academic Press, London (1982).
18. C. Baess and F. Mesmer, "The Hydrolysis of Cations", Wiley–Interscience, New York (1976); A. Clearfield, *in* "Surface Organometallic Chemistry: Molecular Approaches to Surface Catalysis" (J. M. Bassett *et al.*, Eds.), p. 271, Kluwer, 1988.
19. R. W. Kolaczowski and R. A. Plane, *Inorg. Chem.* **3,** 322 (1964); L. Monsted, O. Monsted, and J. Springborg, *Inorg. Chem.* **23,** 2160 (1984).
20. H. Stünzi and W. Marty, *Inorg. Chem.* **22,** 2145 (1983).
21. H. Stünzi, L. Spiccia, F. P. Rotzinger, and W. Marty, *Inorg. Chem.* **28,** 66 (1989).
22. T. Merakis and L. Spiccia, *Aust. J. Chem.* **42,** 1579 (1989) and references therein.
23. H. Stünzi, F. P. Rotzinger, and W. Marty, *Inorg. Chem.* **23,** 2160 (1984).

24. A. J. JACOBSON AND M. S. WHITTINGHAM, (Eds.) "Intercalation Chemistry", Academic Press, New York (1982).
25. A. CLEARFIELD, *in* "Inorganic Ion Exchangers," CRC Press, FL (1982).
26. J. STERTE, *Clays Clay Miner.* **34,** 658 (1986); D. E. W. VAUGHAN, *ACS Symp. Ser.*, **368,** 308 (1988).
27. S. J. MACLACHLAN AND D. M. BIBBY, *J. Chem. Soc. Dalton Trans.*, 895 (1989).
28. R. W. CRANSTON AND F. A. INKLEY, *Adv. Catal.* **9,** 143 (1957).
29. A. LECLOUX AND J. P. PIRARD, *J. Colloid Interface Sci.* **70,** 265 (1978).
30. A. CLEARFIELD, *in* "Design of New Materials", (D. L. Cocke and A. Clearfield, Eds.), p. 121, Plenum, New York (1987); A. Clearfield, *in* "Comments in Inorganic Chemistry," p. 89, Wiley, New York (1990).
31. T. J. PINNAVAIA, in "Chemical Physics of Intercalation", NATO, ASI, Series B, Vol. 172, p. 233.
32. K. S. W. SING, *Pure Applied Chem.* **54,** 201 (1982).
33. A. DYER AND T. GALLARDO, *in* "Recent Developments in Ion Exchange," (P. A. Williams and M. J. Hudson, Eds.) vol. 2, p. 75, Elsevier, London (1990).